Depleting Depletion: Maintaining Single-Walled Carbon Nanotube Dispersions after Graft-to Polymer Functionalization

*Adam J. Clancy,[a,b,c] Hannah S. Leese,[d] Noelia Rubio,[c] David J. Buckley,[c,e] Jake L. Greenfield,[c] Milo S. P. Shaffer[c,] **

a) Department of Chemistry, University College London, London WC1E 7JE, U.K

b) Institute for Materials Discovery, University College London, London WC1E 7JE, U.K

c) Department of Chemistry, Imperial College London, London, SW7 2AZ, U.K.

d) Department of Chemical Engineering, University of Bath, Bath BA2 7AY, U.K.

e) National Physical Laboratory, Teddington, TW11 0LW, U.K.

Email: m.shaffer@imperial.ac.uk

ABSTRACT

Grafting polymers onto single-walled carbon nanotubes (SWCNTs) usefully alters properties but does not typically yield stable, solvated species directly. Despite the expectation of steric stabilization, a damaging (re)dispersion step is usually necessary. Here, poly(vinyl acetate)s

(PVAc) of varying molecular weights are grafted to individualized, reduced SWCNTs at different concentrations to examine the extent of reaction and degree of solvation. The use of higher polymer concentrations leads to an increase in grafting ratio (weight fraction of grafted polymer relative to the SWCNT framework), approaching the limit of random sequentially adsorbed Flory 'mushrooms' on the surface. However, at higher polymer concentrations, a larger percentage of SWCNTs precipitate during the reaction; an effect which is more significant for larger weight polymers. The precipitation is attributed to depletion interactions generated by ungrafted homopolymer overcoming Coulombic repulsion of adjacent like-charged SWCNTs; a simple model is proposed. Larger polymers and greater degrees of functionalization favor stable solvation, but larger and more concentrated homopolymers increase depletion aggregation. By using low concentrations (25 μM) of larger molecular weight PVAc (10 kDa), up to 65% of grafted SWCNTs were retained in solution (at 65 μg mL^{-1}) directly after the reaction.

INTRODUCTION

Single-walled carbon nanotubes (SWCNTs) have superlative mechanical, optical, and electronic properties[1] and have been proposed for a diverse array of applications including (but far from limited to) multifunctional composites,[2] transistors,[3] and drug delivery.[4] However, their poor solubility and tendency to agglomerate are significant hurdles to practical implementation. The functionalization of SWCNT sidewalls is well established as a route to facilitate processing and assembly; in particular, polymers are often used to increase dispersibility, biocompatibility,[5] and composite interfacial properties.[2] Polymers may be synthesized *in situ* directly from an initiating species pre-attached to the SWCNT surface ("*graft-from*" reaction),[6] typically providing dense coverage but an uncertain molecular weight.[7] Alternatively, pre-synthesized (and well

characterized) polymers can be *grafted-to* SWCNTs.[8, 9] In either case, the SWCNTs should be individualized to ensure that the reaction is not limited only to the outer surface of bundles.[10] Prolonged ultrasonication and/or oxidation is typically performed to disperse SWCNTs; however, these processes significantly damage and shorten the SWCNTs and predominantly lead to smaller bundles of SWCNTs, rather than individualized species.[11]

An alternative processing route reduces SWCNTs to form 'nanotubide' anions[12] which spontaneously dissolve in certain polar, aprotic solvents[13] to give purely individualized species, in principle, without damage.[14] While the thermodynamic driving force of nanotubide solvation is the subject of ongoing debate,[15, 16, 17] it is acknowledged that Coulombic repulsion between adjacent nanotubide (poly)anions in solution provides a significant energetic barrier to reagglomeration. The use of N,N-dimethylacetamide (DMAc) as a solvent simplifies nanotubide processing, as it both dissolves nanotubide ions while remaining stable in the presence of strong reducing agents, such as sodium naphthalide (NaNp). A simple equimolar solution of sodium and naphthalene in DMAc is capable of directly dissolving SWCNT powders with high yields.[18] Following this reduction step, the added charge can be used to initiate functionalization reactions, (most commonly with organohalides) to alter dispersibility,[19, 20] crosslink the SWCNTs as gels,[21, 22] or bind composite matrices.[23, 24] As the reaction proceeds, the functionalized SWCNTs (f-SWCNTs) precipitate out of solution, a process usually attributed to removal of the stabilizing Coulombic repulsion, as the reaction consumes the nanotubide's negative charge.[15] However, the grafting stoichiometries (number of SWCNT carbons per grafted moiety) of most functionalization reactions, especially for sterically bulky *graft-to* polymers, imply that only small fraction of the available charge is consumed in the primary reaction; residual charge is known to remain on the SWCNTs after the initial functionalization and is either deliberately or inadvertently removed

3

during subsequent work-up.[25] The reason for the precipitation during grafting (and before discharging) is, therefore, unclear and problematic since air-stable dispersions of polymer-grafted SWCNTs are crucial targets for many applications. Currently, the newly functionalized SWCNTs are usually redispersed, via shear processing steps which can introduce damage. In this sense, unlike thermodynamically stable nanotubide solutions, which form spontaneously, functionalized SWCNTs are typically metastable dispersions. Ideally, the f-SWCNTs would simply remain in solution after the functionalization.
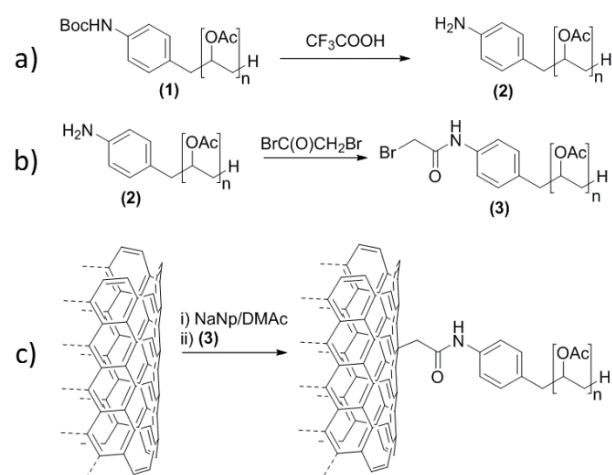

Figure 1. Schematic of polymer end-group functionalization through (a) BOC deprotection and (b) amidation with bromoacetyl bromide, and (c) SWCNT functionalization

METHODS AND EXPERIMENTAL

Materials. Single-walled carbon nanotubes (Elicarb PR929, batch 108511/g) were supplied by Thomas Swan Ltd (U.K.). 4-aminobenzylalcohol (98 %) and 2-bromo-N-phenylacetamide (95%)

were purchased from Fluorochem Ltd. (UK). Di-t-butyl dicarbonate (>99%), pyridine (anhydrous, 99.8%), thionyl chloride (>99%), anhydrous ethanol (200 proof >99.5%), vinyl acetate (>99% with 3-20 ppm hydroquinone stabiliser), trifluoroacetic acid (TFA, 99%), 2,2′-azobis(2-methylpropionitrile) (98%), lauroyl peroxide (Luperox® LP, 97%), sodium (ingot, 99.99%), naphthalene (99%), bromoacetyl bromide (>98%), and anhydrous N,N-dimethylacetamide (99.8%) were purchased from Sigma Aldrich Ltd. (U.K.). Potassium O-ethyl xanthate (98%) was purchased from Alfa Aesar (UK). Dichloromethane (DCM, 99.9%), n-hexane (99.9%), ethanol (96%), tetrahydrofuran (THF, 99.9%), and petroleum benzene (40-60 ºC) were purchased from VWR UK Ltd. (U.K.). Piped nitrogen, and dry oxygen (custom 20/80 v/v oxygen nitrogen mix) were purchased from BOC gases (DE). Anhydrous DMAc was dried further with activated 4 Å molecular sieves (Sigma Aldrich) in a glovebox for 2 days prior to use. Elicarb SWCNTs were purified using a previously reported reductive procedure.[26] Tert-butoxycarbonyl (Boc) protected poly(vinyl acetate) (*1*) synthesis and end-group transformations to aniline (*2*) and bromide (*3*) terminated polymers were performed using previously reported procedures.[27]

Nanotubide Synthesis. Procedure adapted from previously reported literature.[18] Purified nanotubes were dried (10^{-2} mbar, 300 ºC, 1 h) and transferred to a nitrogen glovebox. Separately in the glovebox, a bulk solution of sodium naphthalide in DMAc was prepared by stirring sodium (10 mg) and naphthalene (55.7 mg, 1 eq.) in DMAc (10 mL) using a glass stirrer bar. This solution was stored out of light (covered in aluminium foil), used as soon as possible (maximum 1 week) and monitored for degradation immediately before use, as indicated visually by the appearance of white precipitate and spectroscopically by the reduced intensity of naphthalide's characteristic absorbance band ($\varepsilon_{798\ nm}$ = 26,200 m^{-1} M^{-1} in DMAc). Purified SWCNTs (24 mg) were added to

the NaNp/DMAc solution (4.6 mL), diluted with DMAc (115.4 mL) and stirred with a glass stirrer bar for 16 h to give the nanotubide solution (200 µg mL^{-1}).

Polymer Functionalization. Bromide terminated poly(vinyl acetate) was dissolved in 25 mL DMAc at different concentrations (0.05, 0.5 and 5 mM), set to give final polymer concentrations of 0.025, 0.25 and 2.5 mM. The mixture was injected into a nanotubide solution (25 mL, 200 µg mL^{-1} to give final 50 mL of 100 µg$_{(SWCNT)}$ mL^{-1}) and stirred for 2 h. The solution was then centrifuged (1,000 *g*, 30 min) in fluorinated ethylene propylene (FEP) centrifuge tubes, sealed with PTFE tape in the cap's thread to give a solution and precipitate of f-(PVAc) SWCNTs which were separated by decanting.

Discharging Nanotubide. To remove excess charge, samples were exposed to an atmosphere of dry oxygen overnight. To recover discharged nanotubes for TGA, solutions were filtered over a 100 nm PTFE membrane before washing with deionized water and acetone to remove sodium oxides, naphthalene, and non-grafted polymer. The discharging procedure was also performed on as-dissolved nanotubide solution which was subsequently centrifuged (1,000 *g*, 30 min, in FEP tubes) to give the 'no polymer' control solution (ESI, Fig. S2).

End-Group Only Polymer Functionalization. Nanotubide solution (10 mL, 0.2 mg mL^{-1}, 87 µmol Na) was stirred with 2-bromo-N-phenylacetamide (56 mg, 3 eq. vs Na) with a glass stirrer bar for 16 h, before discharging and filtering over a 100 nm PTFE membrane.

Characterization. UV-Vis spectroscopy was performed on a Perkin Elmer Lambda 950 with an optical glass cuvette, measured with an air background, manually subtracting a measured solvent spectrum afterwards. Concentrations were calculated on post-centrifuged SWCNT-dispersions using an extinction coefficient of ε_{660nm} = 3616.6 mL mg^{-1} m^{-1} calculated previously[26] from mass measurements of undoped SWCNTs. The selected wavelength is away from any

polymer absorption signal, and whilst in principle the extinction coefficient might vary between products, the change is expected to be minor compared to the inherent absorption of SWCNTs, and is known to be consistent with mass filtration and TGA based quantification.[16] TGA was performed on a Perkin Elmer Pyris One under N_2 (60 sccm), holding at 100 °C for 30 min before heating to 700 °C at 10 °C min^{-1}. Grafting ratios were calculated from the weight loss at 700 °C, minus 2.8% (to account for inherent weight loss in the SWCNTs, SI Fig S3c) and multiplied by 1.08 (to account for the 8 wt% ash seen from PVAc degradation, SI Fig S3c) divided by the remaining weight at 700 °C minus the ash content (the aforementioned 8 w t% of weight loss), expressed as a percentage ratio of polymer relative to SWCNT framework. Grafting stoichiometries (C/R) were taken as the ratio of SWCNT carbon atoms (weight percentage SWCNT divided by 12, assuming all weight is carbon framework) to polymer chains (weight percentage polymer divided by M_n). Polymer weights were measured using ^{1}H NMR spectroscopy recorded on a Bruker AV400 (400 MHz) spectrometer, with a CDCl$_3$ (VWR) solution. Spectra were calibrated with the CHCl$_3$ peak and number of monomers calculated from the ratio of backbone hydrogen α to the acetate (4.66-5.10 ppm, nH/monomer) and the less downshifted aromatic protons (7.08 ppm, 2H). Assigned NMR spectra are provided in the supplementary information (SI, Fig S6 – 9). M_n values were verified before use by Polymer Labs GPC 50 system with two PL-gel 5μ columns, calibrated to PMMA standards.

Raman spectroscopy was performed on a Renishaw InVia micro-Raman Spectrometer using a 785 nm laser (1800 nm grating), centered around 1450 cm^{-1} over a 200 × 200 μm grid with 10 μm spacing in a square array (N = 441). Fitting for D/G mode ratios was performed using WiRE 4.1, removal of a linear background followed by peak-fitting D (initial value 1340 cm^{-1}), G$^-$ (1560 cm^{-1}) and G$^+$ (1589 cm^{-1}) modes; values given as ratios of D/G$^+$ intensity. IR spectroscopy was

performed on a Brooker Alpha II Platinum ATR at 4 cm^{-1} resolution for 16 scans using atmospheric compensation. SEM was performed on a Zeiss Leo 1530, with samples mounted to aluminium stubs (Agar Scientific) by carbon tabs (Agar Scientific). Images were taken with an accelerating voltage of 10 keV (unless stated) and post-processed in GIMP (v.2.10.4) to maximize contrast.

RESULTS AND DISCUSSION

Poly(vinyl acetate) (PVAc) was selected as the polymer graft of choice as a precursor to poly(vinyl alcohol) (PVOH), which is used in high performance composites[28] and biomedical applications[29]; PVOH is incompatible with nanotubide functionalization, as the hydroxyl protons hydrogenate the nanotube while consuming charge. Additionally, PVAc is highly soluble in in the nanotubide solvent DMAc.[18] Using previously reported methods,[23] a series of mono-protected-amine (PVAc) molecules were synthesized (**1**) at varying molecular weights: PVAc was selected owing to its high solubility in the nanotubide solvent DMAc. These PVAcs were deprotected to the amine terminated PVAc (**2,** Fig. 1a), and subsequently reacted with bromoacetyl bromide to form mono-bromine-terminated polymers suitable for *grafting-to* nanotubide (**3**, Fig. 1b). Nanotubide solutions were reacted with **3** to form f-SWCNTs (Fig. 1c) to study the influence of varying polymer molecular weight (M_n 500, 5747, and 10517 Da) and concentration (2.5, 0.25 and 0.025 mM).

Thermogravimetric analysis (TGA), relative to controls, determines the grafting ratio (*GR;* weight percentage polymer relative to SWCNT framework carbon). Higher initial polymer concentration clearly correlates with an increased grafting ratio (Fig. 2a), for all molecular weights. As verified previously,[23] all mass loss (relative to a polymer free control sample) observed by TGA can be attributed to grafted polymer and not physisorption. The nanotubes which precipitate during the

8

reaction showed the same grafting ratio as the f-SWCNTs which remained in solution (ESI Fig. S3a) indicating that the SWCNTs which precipitate during the reaction is not due to inhomogeneity in the degree of functionalization. Functionalization was further verified through the Raman D/G mode ratio (ESI Fig. S10), and SEM micrographs (ESI Fig. S11 – 14) which showed no bulk free polymer.
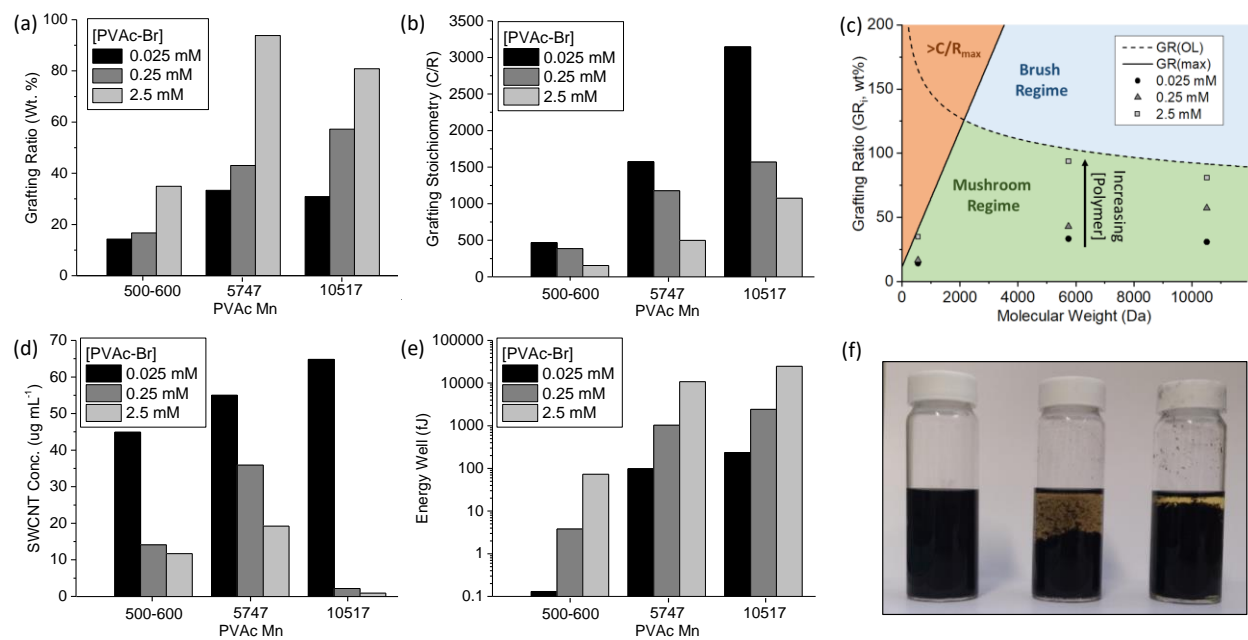

Figure 2. Grafting and retained dispersiblity of f -SWCNTs after reductive functionalization with PVAc-Br of varying molecular weight at varying concentrations. (a) Grafting ratio, (b) Grafting stoichiometry, (c) Grafting ratios versus polymer M_n plotted against grafting limits estimated from maximum utilization of grafting sites (solid line) and de Gennes' surface-adhered polymer theory (dashed line), (d) Concentration of SWCNTs in solution after reductive functionalization with PVAc-Br at varying concentrations, (e) Logarithmic plot of the potential energy well derived from the integral of the interplate pressure versus inter-nanotube distance in the attractive region using

$\mu = 2\pi$ (*i.e.* perpendicular 1 nm diameter SWCNTs). (f) Digital image of the post-reaction mixtures for M_n 10,417 prior to centrifugation at different initial polymer concentrations (from left to right 0.025, 0.25, 2.5 mM). See ESI for raw TGA and UV-vis spectra (ESI Fig. S1).

In general, the relationship between polymer molecular weight and grafting ratio is non-linear, as observed previously for both SWCNTs[23, 30] and other nanocarbons[19] due to two contrasting effects. As polymer weight is increased, firstly, the weight added per chain increases linearly, and secondly, steric occlusion of polymers increases the average distance between grafting sites on the nanotube.

The maximum number of possible grafting sites (C/R_{max}), cannot simply be defined by the carbon/metal stoichiometry. As is typical in the reductive functionalization reaction of SWCNTs, only a small degree of charge was consumed in the reaction,[25, 31] with all grafting stoichiometries (C/R, Fig. 2b) significantly higher than the value of 10 which would correspond to complete charge utilization of the $C_{10}Na$ nanotubide. In principle, there may be a steric effect, depending on the size of the grafted species, and an electronic effect, depending on the availability of electrons with sufficient reducing power to initiate the reaction. The latter limit was estimated by functionalizing the SWCNTs with a polymer containing zero monomers (*i.e.* just the end-group) to find the end-group-only grafting ratio limit. Assuming that every possible reactive site grafts a polymer chain, regardless of molecular weight, the grafting limit in the absence of polymer chain steric occlusion may be calculated. Here, the end-group-only material is 2-bromo-N-phenylacetamide, which gives a C/R_{max} of 156 (ESI Fig. S3b), and an associated GR_{max} that increases linearly with grafted polymer molecular weight (Fig. 2c, solid line).

It has been shown previously that the reductive *graft-to* polymer functionalization of carbon nanomaterials leads to 'mushroom' like behaviour[19, 32] as originally modelled by de Gennes[33] for polymers on surfaces. At higher grafting ratios, the polymer must adopt a stretched 'brush' conformation extending away from the surface. Typically, this morphology only forms via *graft-from* reactions, in which the monomer is added at the growing-chain end, avoiding steric occlusion at the surface. *Graft-to* reactions of pre-synthesized polymers are limited by the steric interactions of the coils, which collapse onto the surface to form a 'mushroom' conformation. The occlusion area of a 'mushroom' polymer in de Gennes' theory is a function of polymer Flory radius (R_F, Eq. 1), which is the product of the length of the monomer (a) and number of monomers (N) to the power of 3/5. The mushroom regime of de Gennes' theory occurs when the average separation between the loci of polymer functionalization is greater than the Flory radius. Treating the polymers as iteratively added hard circles on a plane (with an areal density of carbon atoms, ρ_A, 2.619 Å^{-2}), the packing density can be modelled with random sequential adsorption theory,[34] which has a packing efficiency (η_{RSA}) of 54.7%. Using this efficiency factor along with the Flory radius, the limits due to steric occlusion can be estimated for both the grafting stoichiometry (C/R_{OL}, Eq. 2) and grafting ratio (GR_{OL}, Eq. 3), as a function of polymer molecular weight (Fig. 2c, dashed line):

$$R_F = N^{3/5}a \qquad (1)$$

$$C/R_{OL} = \pi N^{6/5} a^2 \eta_{RSA} \rho_A^{-1} \qquad (2)$$

$$GR_{OL} = \frac{M_w}{12(C/R_{OL})} \qquad (3)$$

During reaction between bromo-terminated polymer and nanotubide, increasing the concentration of polymer increases the grafting ratio towards the maximum grafting limit for all

11

polymer molecular weights, but notably neither the mushroom/brush transition (GR_{OL}, Fig. 2c) nor maximum grafting limit (GR_{max}, Fig 2c) are ever exceeded by the experimental data. However, the concentration of the f-SWCNTs remaining in dispersion after the functionalization (Fig. 2d) does not follow the trend of grafting ratio. There is an inverse relationship between initial polymer concentration and retained dispersibility for all polymer molecular weights, with the highest polymer concentration (2.5 mM) leading to dispersibilities as low as 0.9 µg mL^{-1} (for M_n 10,417), lower even than ungrafted, oxygen-discharged nanotubide (< 10.0 µg mL^{-1}, ESI Fig. S2). On the other hand, low polymer concentrations (0.025 mM) allow a high proportion (65%) of SWCNTs to remain in solution: up to 64. 8 µg mL^{-1} remain from initial loading of100 µg mL^{-1} (72 times higher than the maximum obtained using 2.5 mM PVAc). The dramatic differences in dispersibility occur despite substantially smaller changes in grafting densities (around 50% higher grafting ratios when increasing polymer concentration from 0.025 to 2.5 mM), particularly for the largest polymer (M_n 10,417), indicating that the retained dispersibility must depend on an alternative factor. Further decreases in polymer concentration, at constant SWCNT concentration, are not practical, as the absolute ratio would preclude significant functionalization. For example, at 0.0025 mM 550 Da PVAc, the SWCNT:polymer weight ratio would be 72:1, at the limit of detection even with perfectly efficient grafting. As the intrinsic dispersibilities of isolated PVAc-functionalised SWCNTs of comparable molecular weights are known to be greater than the concentrations seen here (>100 µg mL^{-1} after filtration, washing, and redispersion[27]), the precipitation during the reaction must be attributed to alternative effects during the reaction. Indeed, removing the residual charge from the nanotube dispersions directly after functionalization, by discharging with oxygen, had no effect on dispersed SWCNT concentration, indicating that the dispersions at their post-reaction concentrations were sufficiently stabilized by

12

the grafted PVAc (presumably with higher intrinsic dispersibilites than the concentrations retained during the reaction). Here, the stability of the SWCNTs in solution during the grafting reaction are modelled as a balance between Coulombic repulsion and depletion interactions of solvated polymers. The short-range nature of van der Waals interactions are negligible at the length scales of interest here (>10 nm, *vide infra*) so can be omitted.

Quantifying local forces for rod-like colloids is significantly more complex than the standard adjacent plate or spherical colloid models due to varying orientation of the rods,[35] so here the system is treated with the Derjaguin approximation.[36, 37, 38] A full discussion is provided in the ESI, but in short, cylinders may be treated numerically as linearly related to plate models, multiplied by a coefficient (μ) determined by the radius (R) and angle of interaction of the cylinders. Trends remain constant across all interaction angles and diameters. This assumption requires that cylinders are of equal and constant radius, and the distribution of inter-cylinder angles is stochastic.

The Coulombic repulsion between reduced nanotubes in solution (Π, Eq. 4) is modelled as a superposition[39] of two like-charged nanotubes treated with the electrostatic component of DVLO theory[40] (named for Derjaguin, Landau, Verwey, and Overbeek); dispersive forces are omitted as noted above. The repulsion is a function of surface potential (Ψ_0, Eq. 5), electrolyte concentration (N_T), solvent dielectric constant (ε_r), and temperature (T), inversely exponentially related to inter-nanotube distance (h) and the solvent/temperature-dependent Debye length (κ^{-1}, Eq. 6). As the degree of charging is high, the average charge separation on the SWCNT framework will be below the Bjerrum length (λ_B), and in accordance with Manning-Oosawa (MO) theory,[41] counterions will condense on the charge surface to limit the unshielded surface charge density[42] (σ) to e/λ_B^2 (Eq. 7). As a negligible proportion of the total charge is consumed during functionalization (C/R ≥ 387 from C:Na 10:1), the nanotubide surface charge is assumed to remain within the MO limited

13

regime throughout functionalization. Additionally, it is assumed that the polymer (both adhered

and in solution) does not affect the effective dielectric constant of the electrolyte.

$$\Pi = 2\varepsilon_r\varepsilon_0\kappa^2\Psi_0^2 e^{-\kappa h} \tag{4}$$

$$\Psi_0 = \frac{2k_BT}{ze}\sinh^{-1}\left(\frac{\sigma}{\sqrt{8N_TN_A\varepsilon_r k_BT}}\right) \tag{5}$$

$$\kappa^{-1} = (2e^2z^2N_TN_A\varepsilon_r\varepsilon_0 k_BT)^{-0.5} \tag{6}$$

$$\sigma = \frac{e}{\lambda_B^2} = \frac{16\pi^2\varepsilon_r\varepsilon_0 k_B^2 T^2}{e} \tag{7}$$

Attractive 'depletion interactions' develop between colloidal particles in a dilute polymer

solution due to osmotic effects.[43] Classically, the depletion force (D, Eq. 8) is linearly related to

the number concentration of the polymer (ρ) and occurs when twice the radius of gyration[44] (R_s,

Eq. 9) is greater than the distance between two plates (h), *i.e.* where $2R_S > h$ (Fig. 3a); the Heaviside

function (Θ) ensures repulsion doesn't occur outside this regime. For polymer grafted nanotubes,

the occlusion distance is not equivalent to the inter-SWCNT distance (h) as the additional volume

of the grafted polymer (of radius R_F) on both SWCNTs must be accommodated (Fig. 3) to give a

f-SWCNT specific depletion force (D_{CNT}, Eq. 10).

$$D = \rho k_BT\Theta(2R_S - h) \tag{8}$$

$$R_S = (1/\sqrt{6})N^{1/2}a \tag{9}$$

$$D_{CNT} = \rho k_BT\Theta(2R_S + 2R_F - h) \tag{10}$$
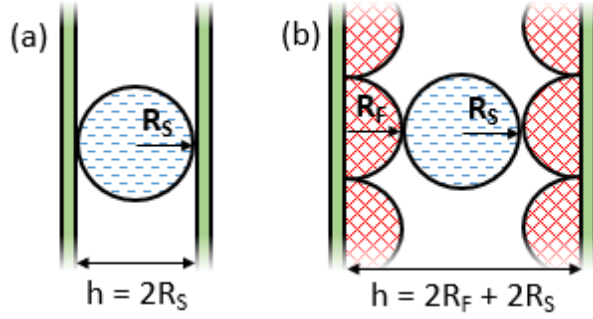
Figure 3. Schematic of depletion interaction onset distance of plates (green) in a solution of free polymer (blue dashed) for (a) plain plates and (b) plates covered in grafted polymer (red cross-hatch)

Here, the inter-SWCNT areal force (F) is treated as the simple combination of the linear depletion force and exponential Coulombic repulsion, each treated with the Derjaguin approximation (Eq. 11–12).

$$F = \mu(\Pi - D_{CNT}) \tag{11}$$

$$F = \frac{2\mu\varepsilon_r\varepsilon_0\kappa^2\Psi_0^2}{e^{\kappa h}} - \mu\rho k_B T\Theta(2R_S + 2R_F - h) \tag{12}$$

At distances that satisfy the relations $2\varepsilon_r\varepsilon_0\kappa^2\Psi^2 e^{-\kappa h} = \rho k_B T\Theta(2R_S + 2R_F - h)$ and $h \approx (2R_S + 2R_{dG})$, the net force is attractive (Fig. 4). Integrating numerically, the inter-nanotube force with respect to distance within this region provides an estimate of the surface-normalised attractive energy (as tabulated in Fig. 2e). Larger free polymers cause stronger depletion forces owing to the higher probability of being excluded from the inter-SWCNT region. By far, the most significant decrease in nanotube dispersiblity is seen for the 10517 Da PVAc, which were calculated to have by far the largest attractive energy wells (Fig. 2e). When polymer concentration is sufficiently low to avoid significant depletion interactions (as calculated here for 0.025 mM PVAc), functionalization with

15

larger molecular weight polymers increases the retained dispersiblity; conversely, at higher concentration, depletion interactions with the free polymer reduce dispersiblity at high molecular weights (Fig. 2d).
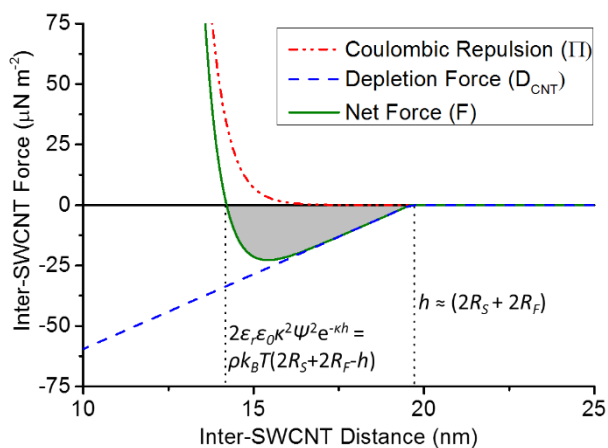

Figure 4. Inter-nanotube pressure versus inter-nanotube distance (green solid) showing contributing Coulombic (red dash-dot) and depletion (blue dash) pressures. Attractive energy well illustrated by grey shading. Distance limits of the attractive well are shown (black dotted) alongside equations. Graph of 2.5 mM 500 Da PVAc shown here; data for all combinations provided in ESI (Fig. S5).

By fixing the concentration and molecular weight of free polymer, the depletion interactions can be kept constant, simplifying studies of other factors. As an example, the kinetics of the grafting reaction as a function of varying end group concentration were studied in this way. For a given total polymer concentration, the proportion of reactive end groups was lowered by adding a 50/50 mixture (M_n 7720 Da) of unreactive Boc-terminated 1 and reactive bromine-terminated 3 to the nanotubide. In comparison to SWCNTs grafted with the same total

16

concentration of only bromine-terminated *3*, the mixed system showed a lower grafting ratio (Fig 5a) and lower dispersability (Fig. 5b). The decreases are attributed to slower grafting kinetics at lower bromide concentration, while the rate of depletion-driven aggregation remains constant; as bundles form, unfunctionalized SWCNTs become occluded. Similar trends are seen at both high and low total polymer concentration, indicating that the availability of reactive end groups affects grafting ratio, as noted above. Where depletion interactions are constant, higher grafting ratio favors retained dispersiblity; however, as before, reducing depletion interactions has a greater effect than increasing grafting ratio (Fig. 5b). The importance of depletion interactions can be seen even in purely non-grafting conditions. Non-grafted, discharged nanotubide yields very low residual levels (10.0 μg mL^{-1}) of metastable dispersed SWCNTs, however, addition of *2* (M$_n$ 5747 Da) at 0.025 mM lowers the f-SWCNT concentration to 6.9 μg mL^{-1}, and removes all measurable SWCNTs from solution at 0.25mM (ESI, Fig. S2b).
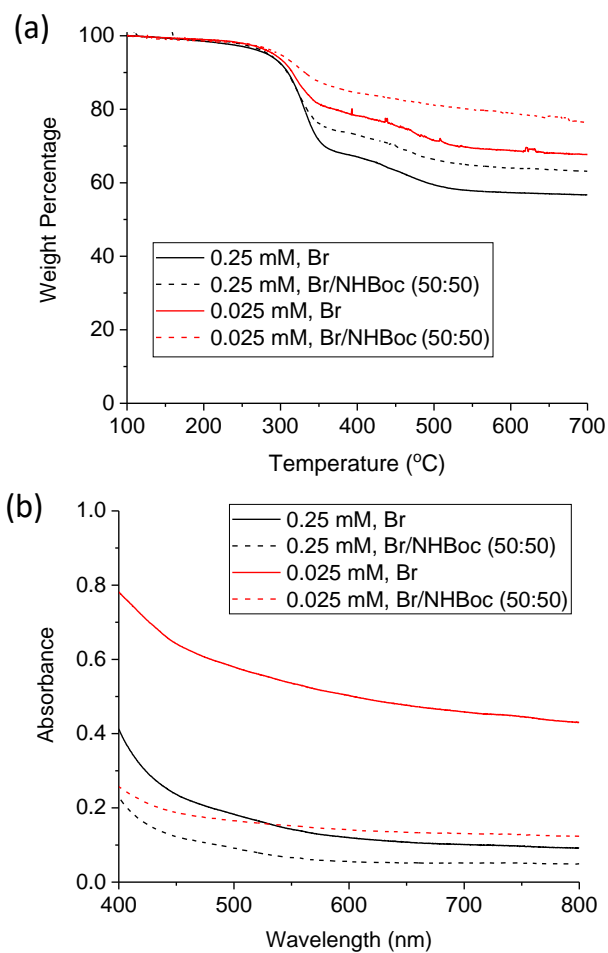
Figure 5. (a) TGA and (b) UV-Vis spectra of SWCNTs mixed with either fully bromide terminated PVAc (solid lines), or an equivalent weight of NHBoc and bromide terminated PVAc, at total polymer concentrations of 0.25 (black), and 0.025 (red) mM.

CONCLUSION

In summary, negatively-charged SWCNT solution behaviors are critically affected by co-solvated polymers, as stabilizing local Coulombic repulsion can be overcome by the osmotic pressure arising from depletion interactions. The interaction between polymer and nanotubide

anions is of particular importance for polymer functionalization reactions where reducing the polymer concentration can be used to curtail depletion interactions and allow the majority of functionalized SWCNTs to remain dispersed. With development, it may be possible to retain the dispersiblity of all the functionalized SWCNTs throughout the reaction. The retained dispersiblity allows further solution processing of the SWCNTs without requiring potentially damaging redispersion techniques. If retaining solvation is of lesser importance compared to maximising grafting, the polymer concentration may be raised to increase grafting ratio, pushing the degree of functionalization towards the de Gennes limit for *graft-to* reactions. This work not only provides a route to f-SWCNT solutions but provides a fundamental framework for a unique system combining classic (polymer) and contemporary (nanotubide) macromolecules. It is likely that the balance between functionalization, depletion and Coulombic repulsion will be seen for other charged, solvated nanomaterials[12] (graphenide, charged transition metal dichalcogenides, nanohorns anions, etc.). Further, it is expected that the same depletion effects will be seen for other polymers with relevance for a range of functionalized SWCNT applications. It is hoped that the simple models demonstrated here may be expanded to predict retained dispersiblity and functionality of a range of functionalized (nano)materials.

SUPPORTING INFORMATION

Raw TGA thermograms, UV-visible spectra, full internatube-interaction energies, full description of Derjaguin approximation, ^{1}H NMR spectra, Raman D/G mode ratios, SEM micrographs, and ATR-IR spectra.

AUTHOR INFORMATION

The manuscript was written through contributions of all authors. All authors have given approval to the final version of the manuscript.

KEYWORDS

Polyvinyl acetate, PVAc, SWCNT, CNT, solution, grafting, individualized, nanotubide

REFERENCES

1.   Hodge, S. A.; Bayazit, M. K.; Coleman, K. S.; Shaffer, M. S. P. Unweaving the Rainbow: A Review of the Relationship Between Single-Walled Carbon Nanotube Molecular Structures and Their Chemical Reactivity. *Chem. Soc. Rev.* **2012,** *41* (12), 4409-4429.
2.   Coleman, J. N.; Khan, U.; Blau, W. J.; Gun'ko, Y. K. Small but Strong: A Review of the Mechanical Properties of Carbon Nanotube–Polymer Composites. *Carbon* **2006,** *44* (9), 1624–1652.
3.   Sgobba, V.; Guldi, D. M. Carbon Nanotubes —Electronic/Electrochemical Properties and Application for Nanoelectronics and Photonics. *Chem. Soc. Rev.* **2008,** *38* (1), 165-184.
4.   Zhang, W.; Zhang, Z.; Zhang, Y. The Application of Carbon Nanotubes in Target Drug Delivery Systems for Cancer Therapies. *Nanoscale Res. Lett.* **2011,** *6* (1), 1-22.
5.   Wang, R.; Cherukuri, P.; Duque, J. G.; Leeuw, T. K.; Lackey, M. K.; Moran, C. H.; Moore, V. C.; Conyers, J. L.; Smalley, R. E.; Schmidt, H. K.; Weisman, B. R.; Engel, P. S. SWCNT PEG-Eggs: Single-Walled Carbon Nanotubes in Biocompatible Shell-Crosslinked Micelles. *Carbon* **2007,** *45* (12), 2388-2393.
6.   Yao, Z.; Braidy, N.; Botton, G. A.; Adronov, A. Polymerization from the surface of single-walled carbon nanotubes− preparation and characterization of nanocomposites. *Journal of the American Chemical Society* **2003,** *125* (51), 16015-16024.

7.   Qin, S.; Qin, D.; Ford, W. T.; Resasco, D. E.; Herrera, J. E. Functionalization of Single-Walled Carbon Nanotubes with Polystyrene via Grafting to and Grafting from Methods. *Macromolecules* **2004,** *37* (3), 752-757.

8.   Li, H.; Cheng, F.; Duft, A. M.; Adronov, A. Functionalization of single-walled carbon nanotubes with well-defined polystyrene by "click" coupling. *Journal of the American Chemical Society* **2005,** *127* (41), 14518-14524.

9.   Liu, Y.; Yao, Z.; Adronov, A. Functionalization of single-walled carbon nanotubes with well-defined polymers by radical coupling. *Macromolecules* **2005,** *38* (4), 1172-1179.

10.   Stephenson, J. J.; Hudson, J. L.; Leonard, A. D.; Price, K. B.; Tour, J. M. Repetitive Functionalization of Water-Soluble Single-Walled Carbon Nanotubes. Addition of Acid-Sensitive Addends. *Chem. Mater.* **2007,** *19* (14), 3491-3498.

11.   Doorn, S. K.; Strano, M. S.; O'Connell, M. J.; Haroz, E. H.; Rialon, K. L.; Hauge, R. H.; Smalley, R. E. Capillary Electrophoresis Separations of Bundled and Individual Carbon Nanotubes. *J. Phys. Chem. B* **2003,** *107* (25), 6063-6069.

12.   Clancy, A. J.; Bayazit, M. K.; S. A. Hodge; Skipper, N. T.; Howard, C. A.; Shaffer, M. S. P. Charged Carbon Nanomaterials: Redox Chemistries of Fullerenes, Carbon Nanotubes, and Graphenes. *Chem. Rev.* **2018,** *118* (16), 7363-7408.

13.   Penicaud, A.; Valat, L.; Derre, A.; Poulin, P.; Zakri, C.; Roubeau, O.; Maugey, M.; Miaudet, P.; Anglaret, E.; Petit, P.; Loiseau, A.; Enouz, S. Mild Dissolution of Carbon Nanotubes: Composite Carbon Nanotube Fibres From Polyelectrolyte Solutions. *Compos. Sci. Technol.* **2007,** *67*, 795–797.

14.   Fogden, S.; Howard, C. A.; Heenan, R. K.; Skipper, N. T.; Shaffer, M. S. P. Scalable Method for the Reductive Dissolution, Purification, and Separation of Single-Walled Carbon Nanotubes. *ACS Nano* **2012,** *6* (1), 54-62.

15.   Voiry, D.; Drummond, C.; Pénicaud, A. Portrait of Carbon Nanotube Salts As Soluble Polyelectrolytes. *Soft Matter* **2011,** *7*, 7998-8001.

16.   Buckley, D. J.; Hodge, S. A.; De Marco, M.; Hu, S.; Anthony, D. B.; Cullen, P. L.; Skipper, N. T.; Shaffer, M. S. P.; Howard, C. A. Trajectory of the Selective Dissolution of Charged Single-Walled Carbon Nanotubes. *J. Phys. Chem. C* **2017,** *121* (39), 21703–21712.

17.   Batista, C. A.; Larson, R. G.; Kotov, N. A. Nonadditivity of Nanoparticle Interactions. *Science* **2015,** *350* (6257), 1242477.

18.   Clancy, A. J.; Melbourne, J.; Shaffer, M. S. P. A One-Step Route to Solubilised, Purified or Functionalised Single-Walled Carbon Nanotubes. *J. Mater. Chem. A* **2015,** *3* (32), 16708-16715.

19.   Rubio, N.; Au, H.; Leese, H. S.; Hu, S.; Clancy, A. J.; Shaffer, M. S. P. Grafting from versus Grafting to Approaches for the Functionalization of Graphene Nanoplatelets with Poly(methyl methacrylate). *Macromolecules* **2017,** *50* (18), 7070-7079.

20.   Voiry, D.; Roubeau, O.; Pénicaud, A. Stoichiometric Control of Single Walled Carbon Nanotubes Functionalization. *J. Mater. Chem.* **2010,** *20*, 4385-4391.

21.   Schirowski, M.; Abellán, G.; Nuin, E.; Pampel, J.; Dolle, C.; Wedler, V.; Fellinger, T. P.; Spiecker, E.; Hauke, F.; Hirsch, A. Fundamental Insights into the Reductive Covalent CrossLinking of Single-Walled Carbon Nanotubes. *J. Am. Chem. Soc.* **2018,** *140* (9), 3352-3360.

22.   De Marco, M.; Markoulidis, F.; Menzel, R.; Bawaked, S. M.; Mokhtar, M.; Al-Thabaiti, S. A.; Basahel, S. N.; Shaffer, M. S. Cross-Linked Single-Walled Carbon Nanotube Aerogel Electrodes via Reductive Coupling Chemistry. *J. Mater. Chem. A* **2016,** *4* (15), 5385-5389.

23.   Clancy, A. J.; Anthony, D. B.; Fisher, S. J.; Leese, H.; Roberts, C. S.; Shaffer, M. S. P. Reductive Dissolution of Supergrowth Carbon Nanotubes for Tougher Nanocomposites by Reactive Coagulation Spinning. *Nanoscale* **2017,** *9*, 8764-8773

24.   Martinez-Rubi, Y.; Ashrafi, B.; Guan, J.; Kingston, C.; Johnston, A.; Simard, B.; Mirjalili, V.; Hubert, P.; Deng, L.; Young, R. Toughening of Epoxy Matrices With Reduced Single-Walled Carbon Nanotubes. *ACS App. Mater. Interf.* **2011,** *3* (7), 2309-2317.

25.   Hof, F.; Bosch, S.; Eigler, S.; Hauke, F.; Hirsch, A. New Basic Insight Into Reductive Functionalization Sequences of Single Walled Carbon Nanotubes. *J. Am. Chem. Soc.* **2013,** *135* (49), 18385–18395.

26.   Clancy, A. J.; White, E. R.; Tay, H.; Yau, H.; Shaffer, M. Systematic Comparison of Conventional and Reductive Single-Walled Carbon Nanotube Purifications. *Carbon* **2016,** *108*, 423-432.

27.   Clancy, A. J.; Serginson, J. M.; Greenfield, J. L.; Yau, H. C.; Shaffer, M. S. P. Systematic Comparison of Single-Walled Carbon Nanotube/ Poly(vinyl Acetate) Graft-to Reactions *Polymer* **2017,** *133*, 263-271.

28.   Lee, W. J.; Clancy, A. J.; Kontturi, E.; Bismarck, A.; Shaffer, M. S. Strong and stiff: high-performance cellulose nanocrystal/poly (vinyl alcohol) composite fibers. *ACS applied materials & interfaces* **2016,** *8* (46), 31500-31504.

29.   Teodorescu, M.; Bercea, M.; Morariu, S. Biomaterials of Poly (vinyl alcohol) and Natural Polymers. *Polymer Reviews* **2018,** *58* (2), 247-287.

30.   Chadwick, R. C.; Khan, U.; Coleman, J. N.; Adronov, A. Polymer Grafting to Single-Walled Carbon Nanotubes: Effect of Chain Length on Solubility, Graft Density and Mechanical Properties of Macroscopic Structures. *Small* **2013,** *9* (4), 552-560.

31.   Hodge, S.; Tay, H.; Anthony, D.; Menzel, R.; Buckley, D.; Cullen, P.; Skipper, N.; Howard, C.; Shaffer, M. Probing the Charging Mechanisms of Carbon Nanomaterial Polyelectrolytes. *Faraday Discuss.* **2014,** *172*, 311-325.

32.   Leese, H. S.; Govada, L.; Saridakis, E.; Khurshid, S.; Menzel, R.; Morishita, T.; Clancy, A. J.; White, E. R.; Chayen, N. E.; Shaffer, M. S. P. Reductively PEGylated Carbon Nanomaterials and Their Use to Nucleate 3D Protein Crystals: A Comparison of Dimensionality. *Chem. Sci.* **2016,** *7* (4), 2916-2923.

33.   de Gennes, P. G. Conformations of Polymers Attached to an Interface. *Macromolecules* **1980,** *13* (5), 1069-1075.

34.   Hinrichsen, E. L.; Feder, J.; Jøssang, T. Geometry of Random Sequential Adsorption. *J. Stat. Phys.* **1986,** *44* (5), 793-827.

35.   Matsuyama, A.; Kato, T. Orientation-Dependent Depletion Interaction in Rodlike Colloid-Polymer Mixtures. *Eur. Phys. J. E* **2001,** *6* (1), 15-24.

36.   Derjaguin, B. Untersuchungen über die Reibung und Adhäsion, IV. *Kolloid-Zeitschrift* **1934,** *69* (2), 155-164.

37.   Israelachvili, J. *Intermolecular and Surface Forces, Second Edition: With Applications to Colloidal and Biological Systems (Colloid Science)*; 2nd Edition ed.; Academic Press1992.

38.   Ohshima, H.; Hyono, A. Electrostatic Interaction Between Two Cylindrical Soft Particles. *J. Colloid Interface Sci.* **2009,** *333* (1), 202-208.

39.   Russel, W. B.; Saville, D. A.; Schowalter, W. R. *Colloidal Dispersions*; 1st Paperback (with corrections) ed.; Cambridge University Press1991.

40.   Ise, N.; Sogami, I. *Structure Formation in Solution: Ionic Polymers and Colloidal Particles*; Springer Science & Business Media2005.

41.   O'Shaughnessy, B.; Yang, Q. Manning-Oosawa Counterion Condensation. *Phys. Rev. Lett.* **2005,** *94* (4), 048302.

42.   Pénicaud, A.; Poulin, P.; Derré, A.; Anglaret, E.; Petit, P. Spontaneous Dissolution of a Single-Wall Carbon Nanotube Salt. *J. Am. Chem. Soc.* **2005,** *127*, 8-9.

43.   Ohshima, Y. N.; Sakagami, H.; Okumoto, K.; Tokoyoda, A. Direct Measurement of Infinitesimal Depletion Force in a Colloid-Polymer Mixture by Laser Radiation Pressure. *Phys. Rev. Lett.* **1997,** *78*, 3963.

44.   Teraoka, I. *Polymer Solutions. An Introduction to Physical Properties*; John Wiley & Sons, Inc: New York, 2002.

For Table of Contents Use Only.
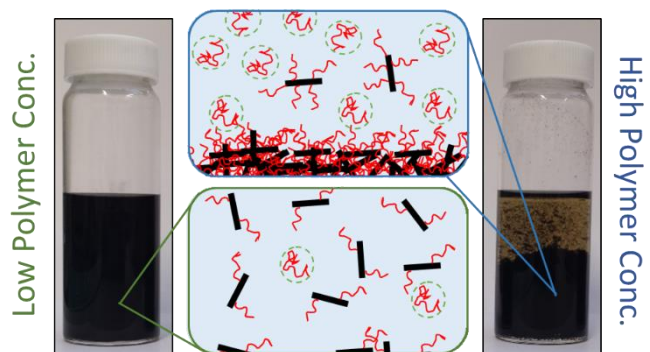
Supporting Information
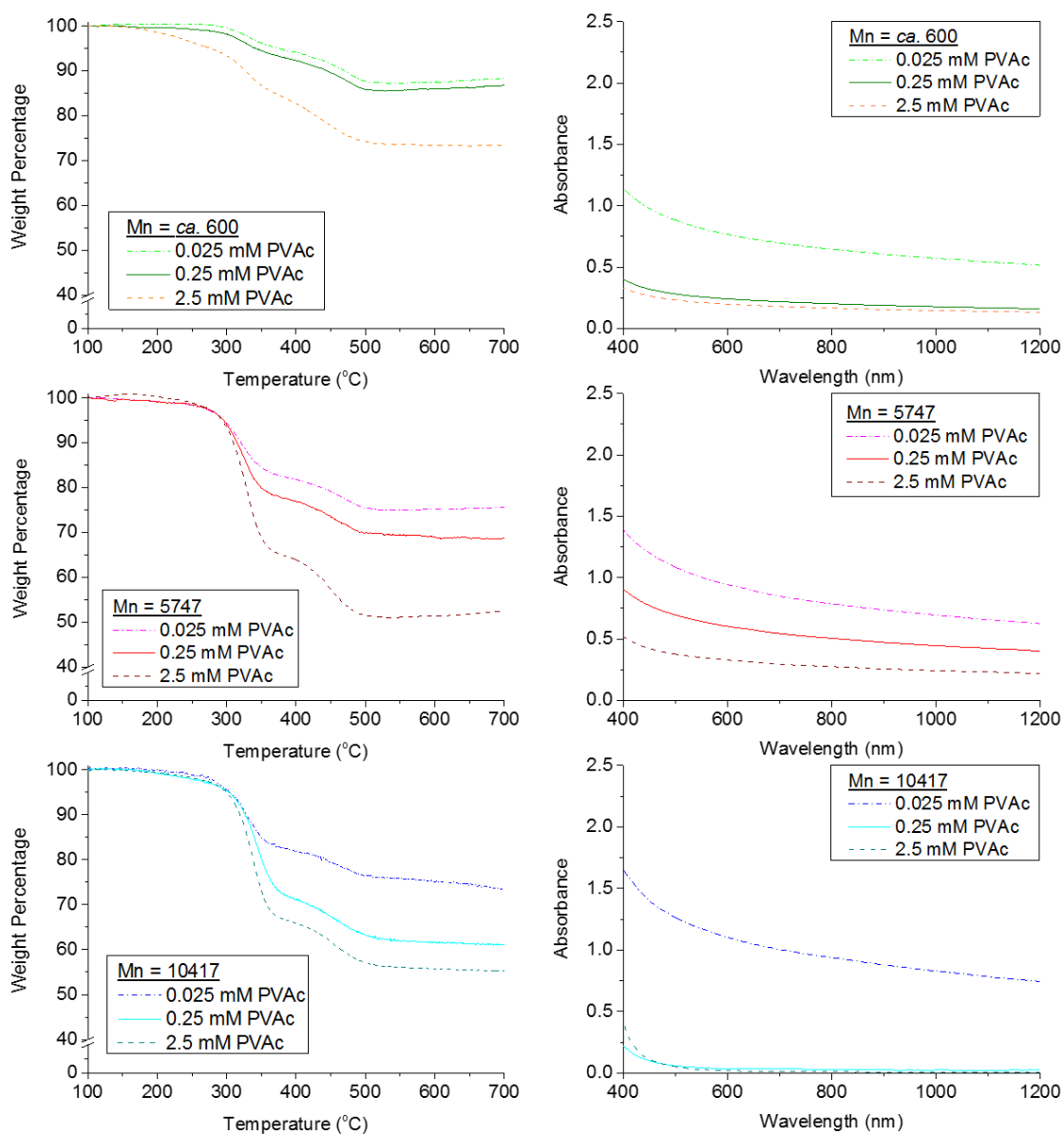
Figure S1. TGA thermograms (Left) and UV-Vis spectra (right) of f-SWCNT and centrifuged post-grafting f-SWCNT solutions at varying polymer concentration for varying molecular weight polymers.
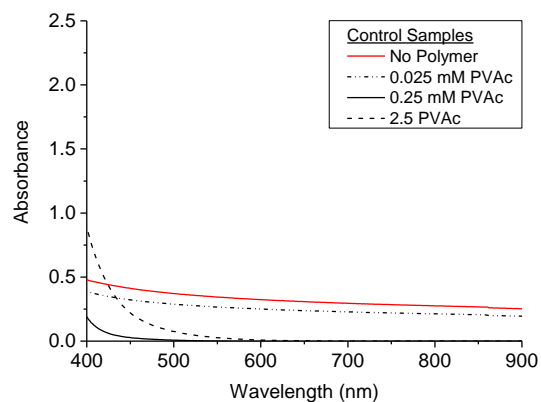
Figure S2. UV-vis spectra of non-grafting control (nanotubide with 2 of differing concentration)
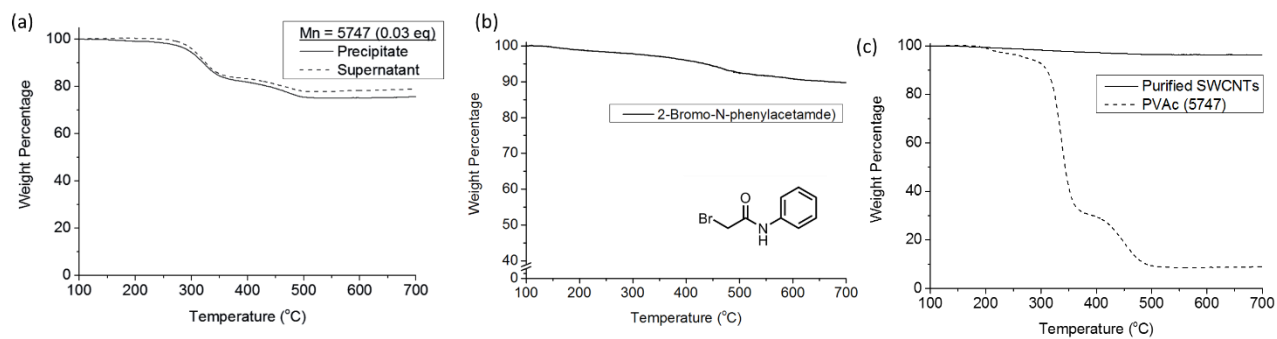
Figure S3. Control TGAs. (a) f-SWCNTs sedimented during centrifugation and filtered from the supernatant. (b) Reaction with polymer end group (**3** with zero monomers) (c) Materials used in the functionalization reaction; polymer (**1** Mn 5747) and purified SWCNTs.
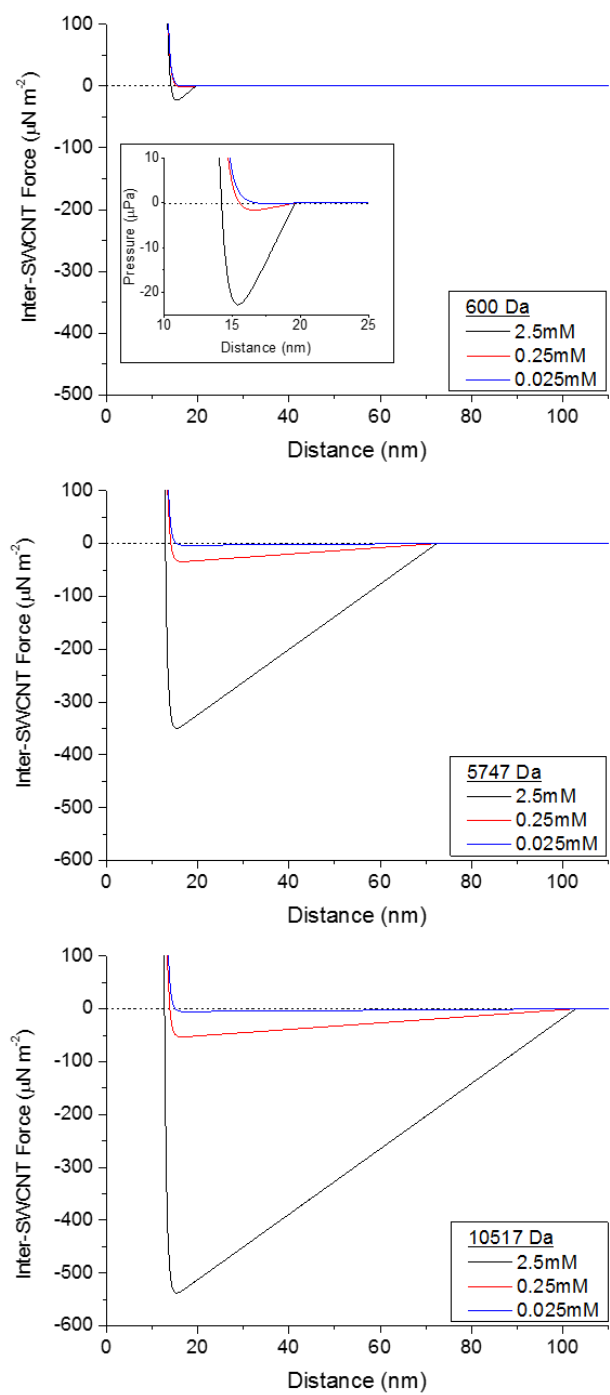
Figure S4. Internanotube interaction energies of all nanotubide/PVAc systems tested here. Intergrals of the attractive regions are presented in the main text (Fig. 2e)

Derjaguin approximation

Accurate quantification of depletion interactions of solutions of stiff rods requires knowledge of the "rod-orientation parameter" which is varies between each SWCNT-SWCNT interaction within a sample. Similarly, there is no analytical solution to the Gouy-Chapman potential model used to calculate Coulombic repulsion of charged rods, only plates and spheres.

Instead, here we use the Derjaguin approximation (Eq. S1, B. Derjaguin, *Kolloid-Zeitschrift*, (1393), **69**, 155-164), a common approximation in colloidal science which models forces between spheres (A_{sphere}) as the force between plates (A_{Plate}) by calculating an effective area of interaction using the effective radius (R_{eff}). The model can be extended to interacting parallel and perpendicular rods (H. Ohshima, *J. Colloid Interf. Sci.*, (2009), **333**, 202-208). Forces between two perpendicular rods ($A\perp$) are treated as interacting spheres (Eq. S2) with effective radius equal to rod radius assuming both rods have identical radii, (Eq. S3). Forces between parallel equal, infinitely long rods ($A_{//}$) can be treated as plates, but with rod-radius-dependent coefficient ($R^{0.5}$, Eq S4). There is currently no exact solution of non-parallel, non-perpendicular rods, although it can be seen that as rods are rotated from parallel to perpendicular, the total area of interaction decreases, and dependence on radii increases. In all cases, the inter-rod force (A_{rod}) is simply the plate model multiplied by a coefficient (μ, Eq. S5) with all values lying between the $A\perp$ and $A_{//}$ limits ($2\pi R < \mu < \sqrt{R}$).

$$A_{sphere} = 2\pi R_{eff} A_{Plate} \tag{S1}$$

$$A_{\perp} = 2\pi R_{eff} A_{Plate} \tag{S2}$$

$$R_{eff} = \sqrt{R_1 R_2} = R \ (when \ R_1 = R_2) \tag{S3}$$

$$A_{//} = \sqrt{\frac{2R_1 R_2}{R_1 + R_2}} A_{Plate} = \sqrt{R}(A_{Plate}) \ (when \ R_1 = R_2) \tag{S4}$$

$$A_{rod} = \mu A_{Plate} \tag{S5}$$

$$F = \mu\Pi + \mu D_{CNT} = \mu(\Pi + D_{CNT}) \tag{S6}$$

Here, the interaction force between adjacent charged nanotubes (F) is approximated as the charge repulsion (Π) plus depletion attraction (D_{CNT}), and each constituent force is treated with the Derjaguin approximation (Eq. S6). So long as μ (and the distribution of per-cylinder-interaction μ's within a system) remains constant, then trends between experiments may be compared regardless of which value is selected for μ; both parallel ($\mu = \sqrt{R}$) and perpendicular ($\mu = 2\pi R$) nanotubes give the same trends (Fig. S7). To maintain the 'constant μ' assumption, it must be assumed that the rod diameters do not change (e.g. trends may not be compared between SWCNT batches where diameter distributions will vary), and the distribution of cylinder interaction angles is unchanged between experiments and conditions, e.g. are stochastic. In the

main text, values for 1 nm perpendicular rods are used; it should be noted that the true values will be numerically larger due to other crossing angles.
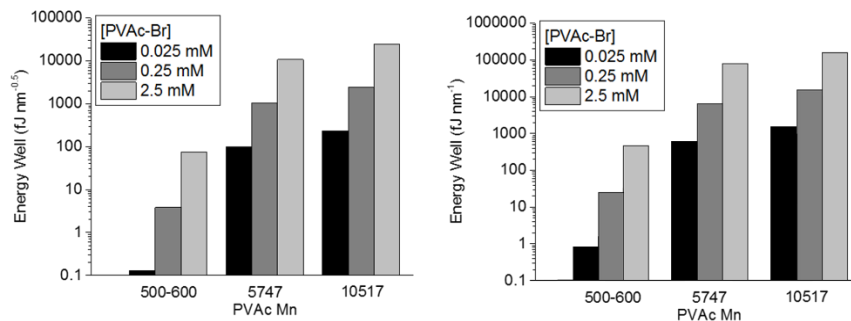

Fig S5. Integrated energy wells for (left) parallel and (right) perpendicular SWCNTs (of 1 nm diameter) showing identical trends, offset by a constant coefficient of π.
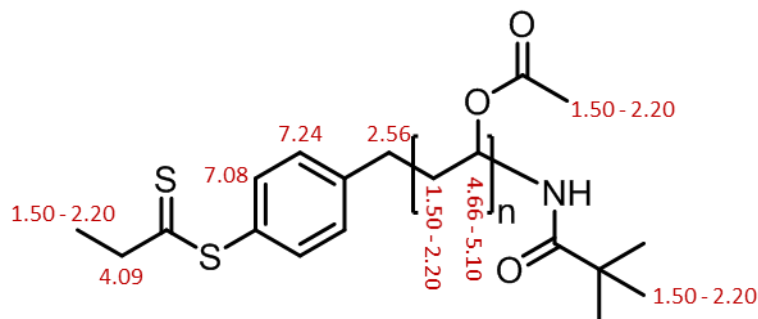
Figure S6. Assignment of proton chemical shifts of as-synthesized xanthate/NBoc asymmetrically terminated polymers (as seen in Fig S7-S9). Aliphatic region (1.5 – 2.20 ppm): BOC protecting group (9H, s), terminal xanthate ethyl hydrogens (3H, t), PVAC CH_2 backbone units (2nH, m), and acetate methyl (3nH, s). δ 2.56, Backbone CH_2 α to aromatic (2H, m). δ 4.09, xanthate methyl (2H, q). δ 4.66-5.10, (2nH, m). δ 7.08 aromatic ortho to xanthate (2H, d). δ 7.24 aromatic ortho to polymer (overlapping with $CHCl_3$ solvent peak, 2H). Monomers for M_n calculated by double the integral of the 4.66-5.10 peaks divided by the integral of the 7.08 peak. Spectra integrals normalized to 7.08 peak.
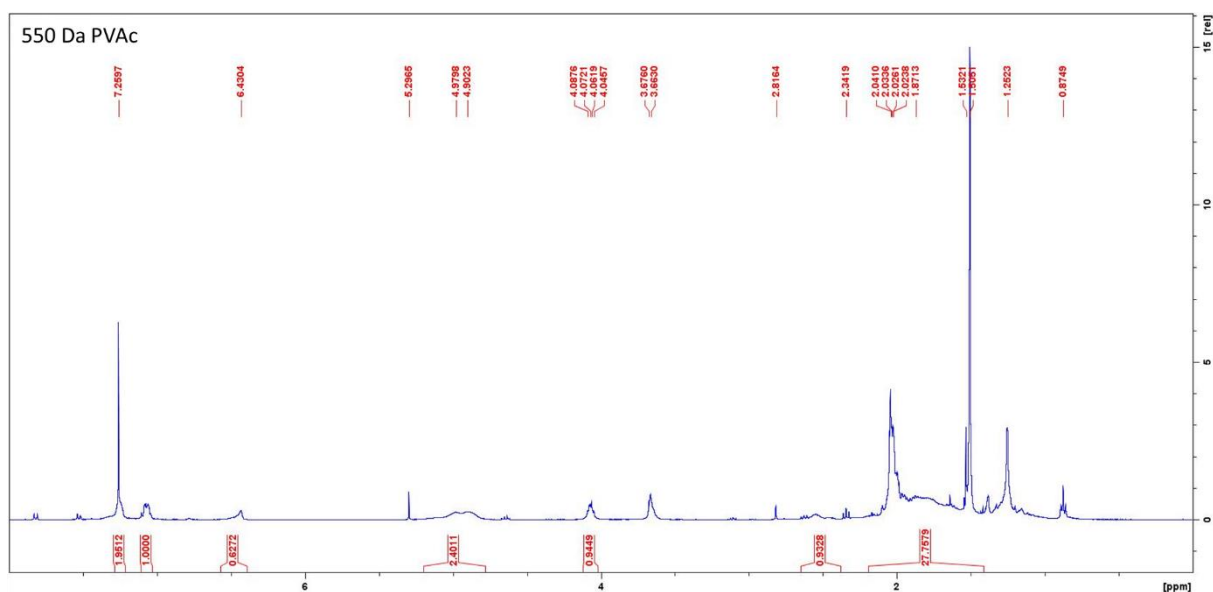
Figure S7. ^{1}H NMR spectra of 500-600 Da as-synthetized PVAc (in CDCl$_3$), 4.7 monomers.
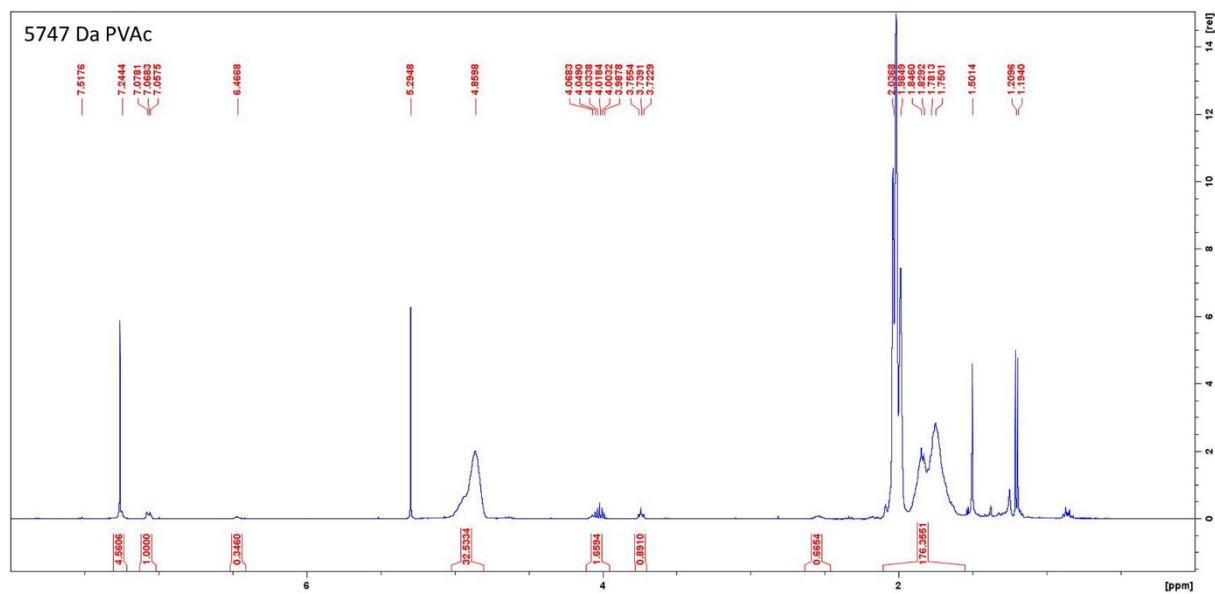
Figure S8. ^{1}H NMR spectra of 5747 Da as-synthetized PVAc (in CDCl$_3$), 65.1 monomers
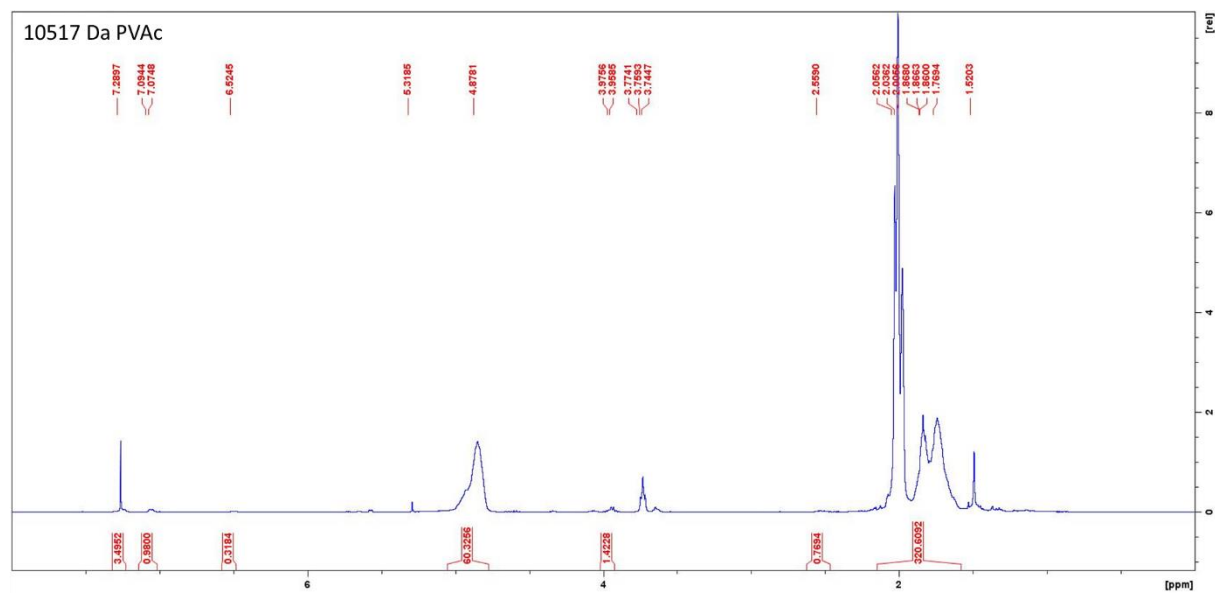


Figure S9. ^{1}H NMR spectra of 10517 Da as-synthetized PVAc (in CDCl$_3$), 120.6 monomers.
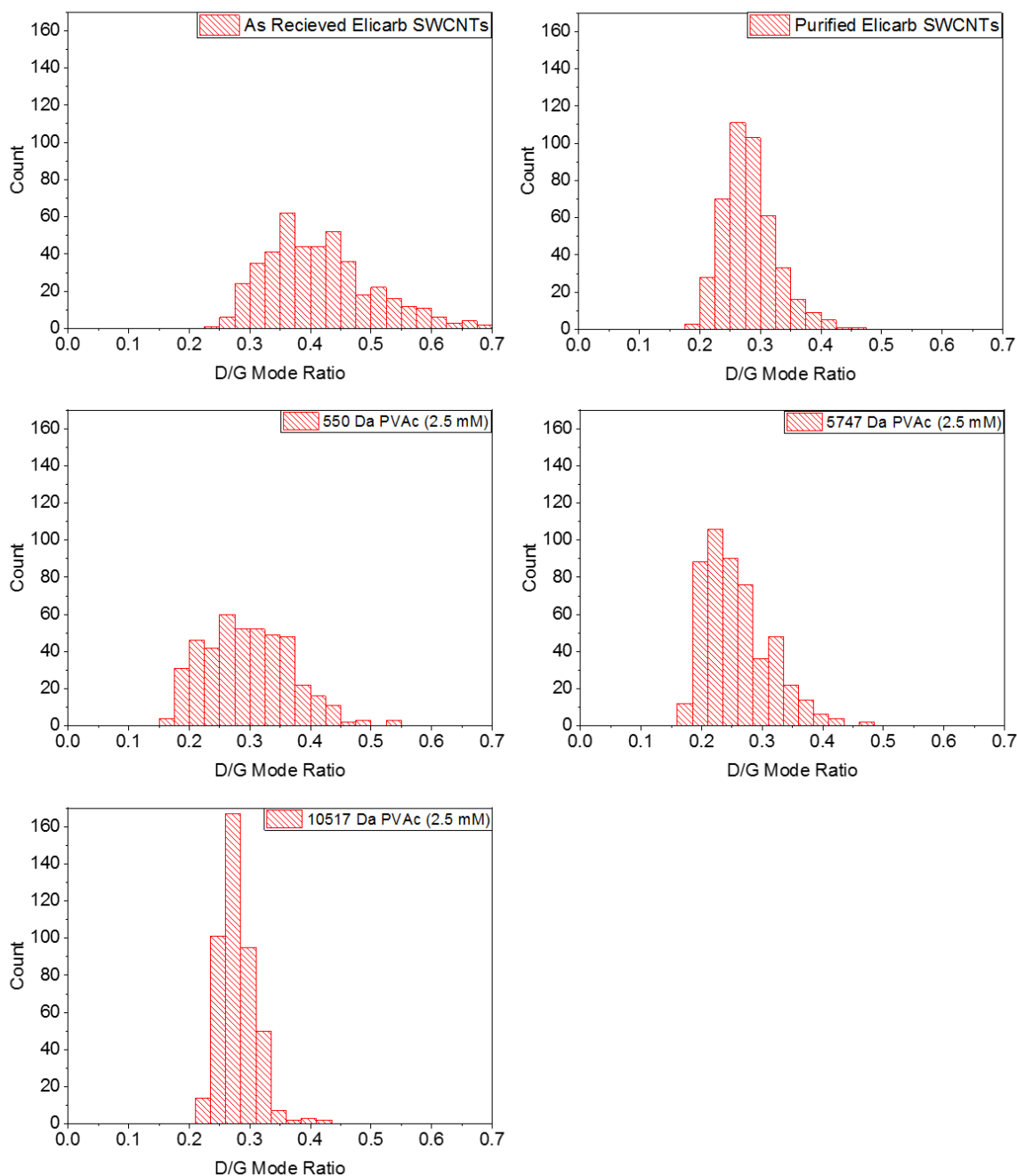
Figure S10. Raman D/G mode ratios for as received, purified, and functionalized SWCNTs (N = 441, in square 200 μm length grid, separated by 10 μm intervals). Increases scale with increasing grafting stoichiometry as expected, with the largest polymer (C/R 1075) showing negligible change.

Figure S11. SEM micrographs of as received SWCNTs
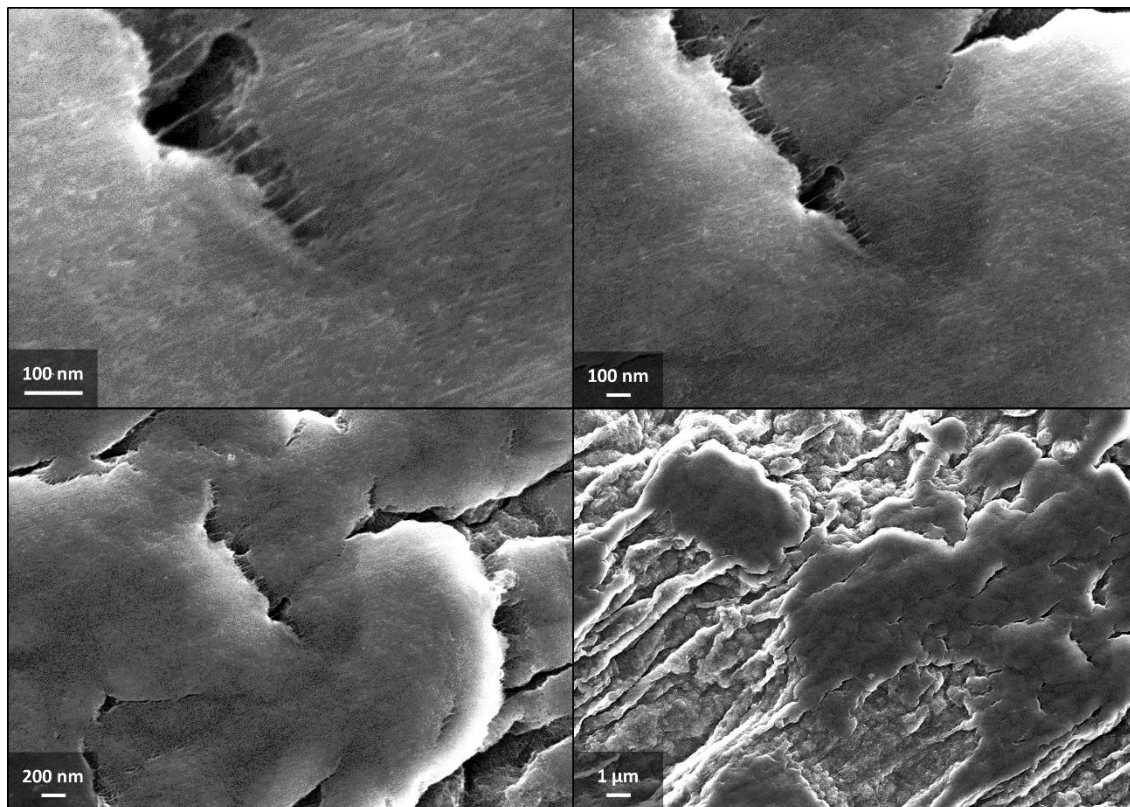
Figure S12. SEM micrographs of SWCNTs functionalized with 550 Da PVAc (2.5 mM, images taken at 5 keV accelerating voltage)
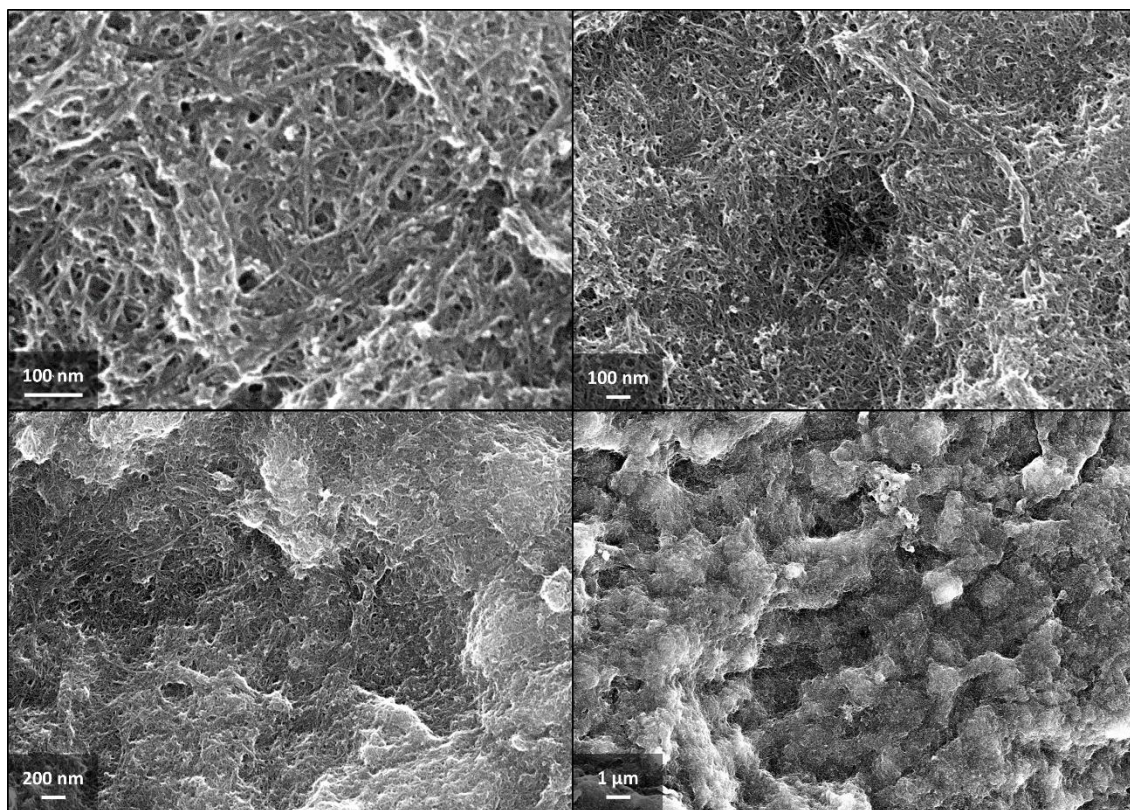
Figure S13. SEM micrographs of SWCNTs functionalized with 5747 Da PVAc (2.5 mM)
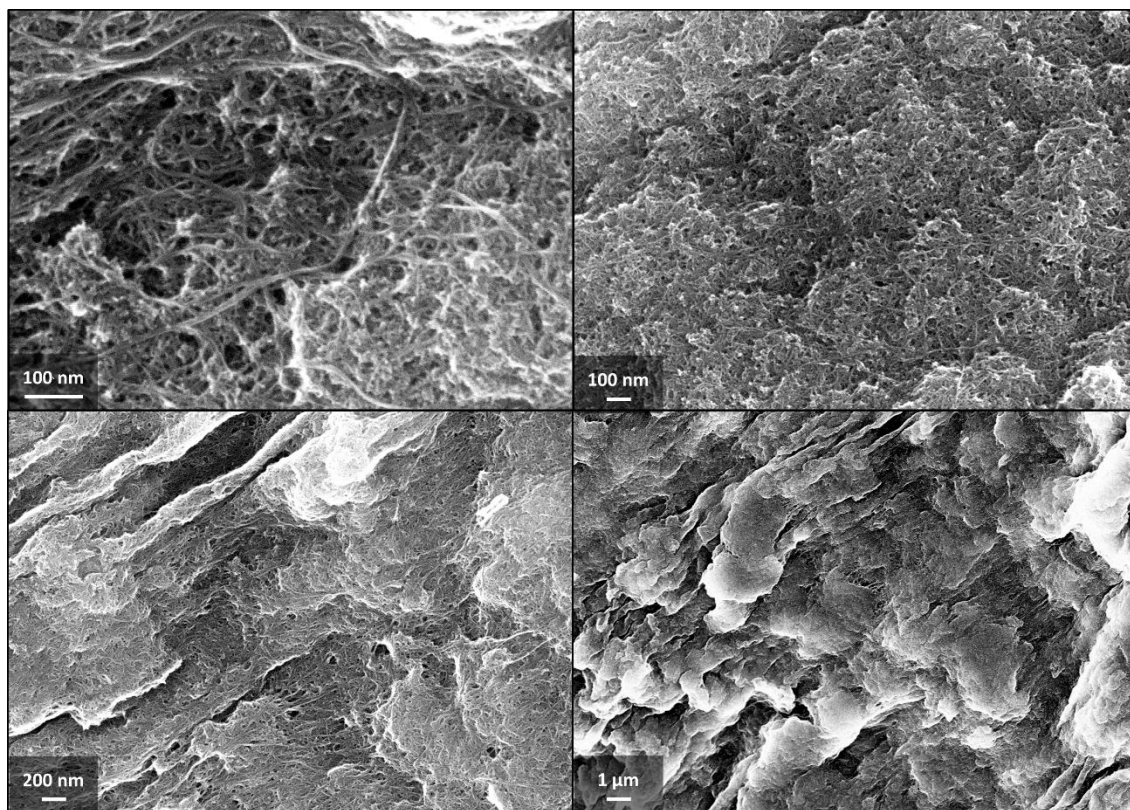
Figure S14. SEM micrographs of SWCNTs functionalized with 10517 Da PVAc (2.5 mM)
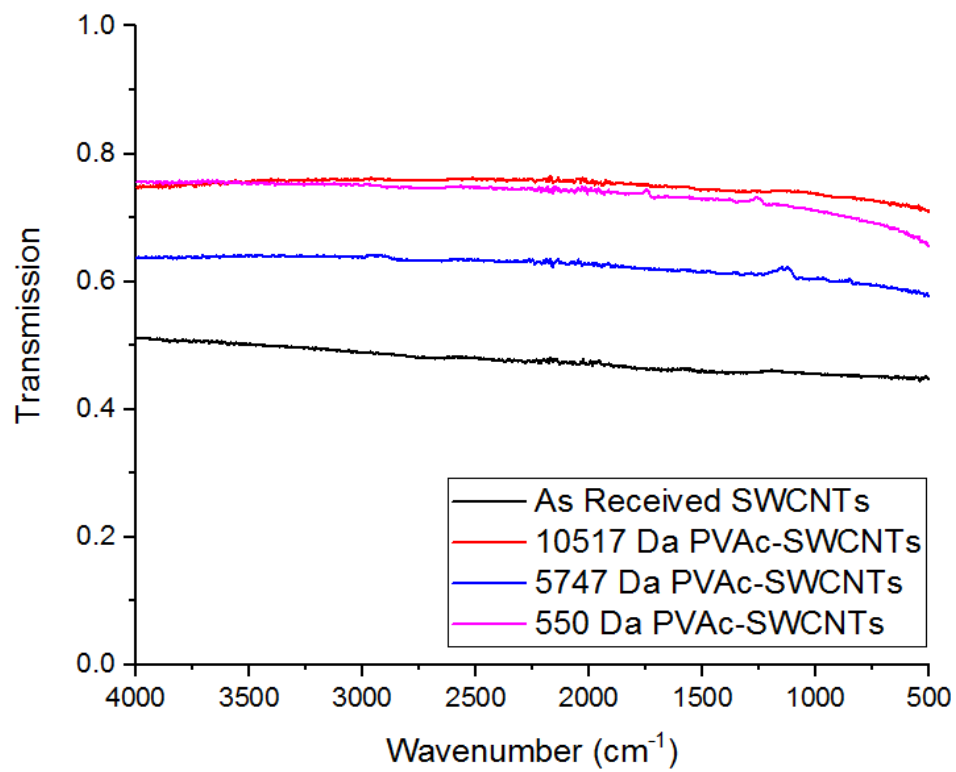
Figure S15. ATR-IR spectroscopy of as received and PVAc functionalized (2.5 mM) SWCNTs.